

Liquid metal expulsion during laser spot welding of 304 stainless steel

X He¹, J T Norris², P W Fuerschbach² and T DebRoy¹

¹ Department of Materials Science and Engineering, Pennsylvania State University, University Park, PA 16802, USA

² Joining and Coating Department, Sandia National Laboratories, Albuquerque, NM 87185, USA

Received 14 September 2005, in final form 15 September 2005

Published 20 January 2006

Online at stacks.iop.org/JPhysD/39/525

Abstract

During laser spot welding of many metals and alloys, the peak temperatures on the weld pool surface are very high and often exceed the boiling points of materials. In such situations, the equilibrium pressure on the weld pool surface is higher than the atmospheric pressure and the escaping vapour exerts a large recoil force on the weld pool surface. As a consequence, the molten metal may be expelled from the weld pool surface. The liquid metal expulsion has been examined both experimentally and theoretically for the laser spot welding of 304 stainless steel. The ejected metal droplets were collected on the inner surface of an open ended quartz tube which was mounted perpendicular to the sample surface and co-axial with the laser beam. The size range of the ejected particles was determined by examining the interior surface of the tube after the experiments. The temperature distribution, free surface profile of the weld pool and the initiation time for liquid metal expulsion were computed based on a three-dimensional transient heat transfer and fluid flow model. By comparing the vapour recoil force with the surface tension force at the periphery of the liquid pool, the model predicted whether liquid metal expulsion would take place under different welding conditions. Expulsion of the weld metal was also correlated with the depression of the liquid metal in the middle of the weld pool due to the recoil force of the vapourized material. Higher laser power density and longer pulse duration significantly increased liquid metal expulsion during spot welding.

1. Introduction

Pronounced vapourization of metal vapours from the weld pool surface occurs when very high power-density energy sources such as laser and electron beams are used for welding [1–8]. If the weld pool temperatures are very high, the escaping vapour exerts a large recoil force on the weld pool surface and, as a consequence, liquid metal droplets may be expelled from the weld pool. In some materials processing operations, such as laser drilling or cutting, liquid metal expulsion is desirable. On the other hand, for several important metal processing operations such as welding, surface alloying and cladding, the metal loss can adversely affect the weld geometry and weldment properties, and liquid weld metal expulsion is undesirable. Therefore, it is important to understand various

factors that affect liquid metal expulsion during high power laser beam welding.

Most of the previous work on liquid metal expulsion has been focused on laser drilling. Voisey *et al* [9, 10] found that the extent to which liquid expulsion occurs depends both on material properties and laser parameters. Two complementary methods, high speed photography and a particle stream interruption technique, were used to determine the ejection velocity. It was shown that increasing the power density increased the ejection velocity. The typical particle diameters appeared to be of the order of the molten layer thickness during drilling. Lu *et al* [11] developed a method to ‘capture’ the particles ejected from the substrate due to laser irradiation. They found that the particles from a smooth substrate concentrated mostly on the centre of the capturing

surface, while those from a rough surface were ejected in more random directions. Yilbas [12] investigated the propagation velocity of the liquid–vapour interface during the laser–metal interaction using a special photographic technique for four metals: titanium, tantalum, nickel and EN58B stainless steel. It was found that the particle velocity at a given laser output energy increased with the decrease in the thermal diffusivity of the material, and particle velocity increased with the increase in laser energy. Rodden *et al* [13] measured the percentage of mass removed as liquid metal expulsion to be 90% for titanium during single pulse Nd:YAG laser drilling. High-speed photographs indicated that there were two distinct stages of liquid metal expulsion during drilling with pulsed laser. There was an initial expulsion of small liquid particles, followed by the expulsion of larger particles of liquid near the end of the pulse.

Liquid metal expulsion has also been studied theoretically. von Allmen and Blatter [14] suggested that vapour pressure acts like a piston that exerts a pressure onto the melt, squirting it out of the melt pool radially. He also developed a theoretical model to calculate drilling velocity and drilling efficiency as a function of the absorbed intensity [15]. Chan and Mazumder [16] developed a one-dimensional steady state model to describe the laser induced damage caused by materials removal through vapourization and liquid metal expulsion. Results were obtained for three materials: aluminum, superalloy and titanium. For the power levels investigated, the material-removal rates were of the order of 1 m s^{-1} and increased with heat-flux intensity. Depending on the materials and beam power density, either vapourization or liquid expulsion was thought to be the dominant mechanism of material removal.

For laser welding, liquid metal expulsion is not desirable, especially for microwelding where the operation is often carried out in a clean room environment after the components have undergone significant prior processing. Basu and DebRoy [17] examined the conditions for the initiation of liquid metal expulsion during laser irradiation experimentally and theoretically. They proposed that liquid metal expulsion takes place when the vapour recoil force exceeds the surface tension force of the liquid metal at the periphery of the weld pool. Semak *et al* [18] assumed that keyhole propagation was dominated by evaporation-recoil-driven melt expulsion from the beam interaction zone. The role of recoil pressure in energy balance during laser material processing was analysed theoretically by Semak and Matsunawa [19].

The work presented in this article was conducted to understand the liquid metal expulsion experimentally and theoretically. During experiments, an open ended quartz tube was placed co-axial to the laser beam and right above the 304 stainless steel samples to collect vapourized elements and ejected metal droplets on the interior surface of the tube. For theoretical work, the temperature field used to simulate liquid metal expulsion was obtained from a well-tested comprehensive three-dimensional transient numerical model. Conditions for the initiation of liquid metal expulsion during laser spot welding of 304 stainless steel were examined by comparing the vapour recoil force with the surface tension force at the periphery of the liquid pool. The free surface profile was simulated at different times by minimizing the total

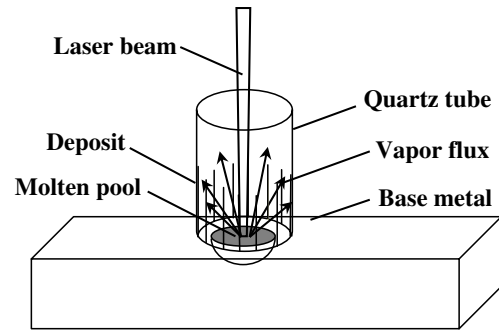


Figure 1. A schematic diagram of the experimental set-up.

surface energy. The prediction from the model whether liquid metal expulsion takes place was compared with experimental observations under different welding conditions.

2. Experimental procedure

Several 304 stainless steel welds were fabricated at the Sandia National Laboratories. The steel had the following composition: 1 wt% Mn, 18.1 wt% Cr, 8.6 wt% Ni, 0.69 wt% Si, 0.046 wt% C, 0.012 wt% P, 0.003 wt% S and balance Fe. A Raytheon model SS 525 pulsed Nd:YAG laser with a 100 mm focal length lens was used for laser spot welding with pulse energies in the range of 2.1–5.9 J and pulse durations of 3.0 ms and 4.0 ms, respectively. Individual spot welds from a pulsed laser beam were made on $3 \times 10 \times 17 \text{ mm}^3$ samples. Up to 15 individual spot welds were made on each of the samples, using a single pulse for each individual spot weld.

A schematic diagram of the experimental set-up is presented in figure 1. During laser spot welding, an open ended quartz tube, 25 mm in length, having a 6 mm inner diameter and a 1 mm wall thickness, was placed co-axial to the laser beam and right above the 304 stainless steel samples. A portion of the vapourized elements and ejected metal droplets were collected on the interior surface of the tube. The deposit and the particles were examined from each experiment. The SEM micrographs and EDS (energy-dispersive x-ray spectroscopy) analysis were performed on the interior surface of the quartz tube for every experiment.

3. Mathematical modelling

3.1. Transient temperature profiles

The temperature profile was calculated using a well tested three-dimensional comprehensive transient heat transfer and fluid flow model. The weld metal was assumed to be an incompressible, Newtonian fluid. Constant thermophysical properties, such as viscosity, thermal conductivity and specific heat, were used for the calculations. The variation of absorption coefficient of the laser energy by the stainless steel at different temperatures was ignored for simplicity. The liquid flow in the weld pool is driven mainly by the Marangoni force resulting from the spatial gradient of surface tension, and to a much lesser extent, by the buoyancy force resulting from the spatial variation of density. The following equations were solved with the appropriate boundary conditions.

Mass conservation:

$$\frac{\partial(\rho u_i)}{\partial x_i} = 0. \quad (1)$$

Momentum conservation:

$$\rho \frac{\partial u_j}{\partial t} + \rho \frac{\partial(u_i u_j)}{\partial x_i} = \frac{\partial}{\partial x_i} \left(\mu \frac{\partial u_j}{\partial x_i} \right) + S_j. \quad (2)$$

Energy conservation:

$$\rho \frac{\partial h}{\partial t} + \rho \frac{\partial(u_i h)}{\partial x_i} = \frac{\partial}{\partial x_i} \left(\frac{k}{C_p} \frac{\partial h}{\partial x_i} \right) - \rho \frac{\partial(\Delta H)}{\partial t} - \rho \frac{\partial(u_i \Delta H)}{\partial x_i}, \quad (3)$$

where ρ is the density, t is the time, x_i is the distance along the $i = 1, 2$ and 3 directions, u_j is the velocity component along the j direction, μ is the effective viscosity, k is the thermal conductivity, C_p is the specific heat, h is the sensible heat, ΔH is the latent heat, and S_j is the source term for the j th momentum equation and is given as:

$$S_j = -\frac{\partial p}{\partial x_j} + \frac{\partial}{\partial x_j} \left(\mu \frac{\partial u_j}{\partial x_j} \right) - C \left(\frac{(1-f_l)^2}{f_l^3 + B} \right) u_j + \rho g \beta (T - T_{\text{ref}}), \quad (4)$$

where p is the pressure, f_l is the liquid fraction, B is a very small positive constant introduced to avoid division by zero, C is a constant that takes into account mushy zone morphology [20], β is the coefficient of volume expansion and T_{ref} is a reference temperature.

The governing equations were discretized and solved iteratively on a line-by-line basis using a tri-diagonal matrix algorithm. The discretized equations for a variable are formulated by integrating the corresponding governing equations over the control volume in a rectangular computation domain. The detailed procedure to solve the equations is described in the literature [21]. After obtaining the values of the sensible enthalpy, h , on computational domain, temperature can be expressed as

$$T = \begin{cases} T_{\text{solid}} + \frac{h - H_{\text{melt}}}{C_{\text{ps}}} & \text{for } h \leq H_{\text{melt}} \\ T_{\text{solid}} + \frac{h - H_{\text{melt}}}{C_{\text{pa}}} \\ = T_{\text{solid}} + \frac{h - H_{\text{melt}}}{H_{\text{cal}} - H_{\text{melt}}} (T_{\text{liquid}} - T_{\text{solid}}) \\ = T_{\text{solid}} + f_l \times (T_{\text{liquid}} - T_{\text{solid}}) \\ \text{for } H_{\text{melt}} < h < H_{\text{cal}} \\ T_{\text{liquid}} + \frac{h - H_{\text{cal}}}{C_{\text{pl}}} & \text{for } h \geq H_{\text{cal}}, \end{cases} \quad (5)$$

where T_{solid} and T_{liquid} are the solidus and liquidus temperature of the material, respectively. H_{melt} is the total enthalpy at the liquidus temperature, C_{ps} and C_{pl} are the specific heat of solid and liquid, respectively. The specific heat, C_{pa} , in the mushy zone was calculated by

$$C_{\text{pa}} = (C_{\text{ps}} + C_{\text{pl}})/2. \quad (6)$$

H_{cal} is given as

$$H_{\text{cal}} = H_{\text{melt}} + C_{\text{pa}} \times (T_{\text{liquid}} - T_{\text{solid}}). \quad (7)$$

Table 1. Data used for calculations [24–28].

Property/Parameter	Value
Density of liquid metal (kg m^{-3})	7.2×10^3
Absorption coefficient	0.27
Effective viscosity ($\text{kg m}^{-1} \text{s}$)	0.1
Solidus temperature (K)	1697
Liquidus temperature (K)	1727
Enthalpy of solid at melting point (J kg^{-1})	1.20×10^6
Enthalpy of liquid at melting point (J kg^{-1})	1.26×10^6
Specific heat of solid ($\text{J kg}^{-1} \text{K}$)	711.8
Specific heat of liquid ($\text{J kg}^{-1} \text{K}$)	837.4
Thermal conductivity of solid ($\text{J m}^{-1} \text{s K}$)	19.26
Effective thermal conductivity of liquid ($\text{J m}^{-1} \text{s K}$)	209.3
Temperature coefficient of surface tension ($\text{N m}^{-1} \text{K}$)	-0.43×10^{-3}
Coefficient of thermal expansion	1.96×10^{-5}
Surface tension coefficient (N m^{-1})	1.872

The boundary conditions, grid spacing, time step, convergence criteria and other details have been described in detail in recent papers [22, 23] and are not repeated here. The computed temperature fields were then used to calculate the vapour pressure. The data used for calculations [24–28] are presented in table 1.

3.2. Free surface profile

When the temperature is very high, the liquid pool severely deforms due to the recoil pressure exerted by the escaping vapour. The calculation of the free surface profile of the weld pool involves minimizing the total surface energy. The total energy includes the surface tension energy for the change in the area of pool surface, potential energy in the gravitational field and the work done by the recoil force. The total energy can be expressed as

$$E_t = \iint_s \left(\gamma \sqrt{1 + \phi_x^2 + \phi_y^2} - \frac{1}{2} \rho g \phi^2 - \Delta P \phi \right) dx dy, \quad (8)$$

where s indicates the surface of the weld pool. On the right hand side, the three terms within the parentheses represent surface energy, potential energy and the work by the recoil force, respectively. The symbol ϕ is defined as the vertical elevation of the top surface with respect to an arbitrarily chosen horizontal plane and depends on x and y . The variables ϕ_x and ϕ_y represent the partial derivatives of ϕ with respect to x and y , γ is the surface tension, ρ is the density and ΔP is the difference between the local equilibrium vapour pressure and the atmospheric pressure. The equilibrium vapour pressure data used for the calculations are available in [8]. In the calculation, the total volume of the liquid pool prior to the liquid metal expulsion is assumed to be constant, so the constraining equation is

$$\Delta V = \iint_s \phi dx dy = 0. \quad (9)$$

4. Results and discussion

Figure 2 shows the presence of condensed metal vapour and ejected tiny droplets on the interior wall of the quartz placed

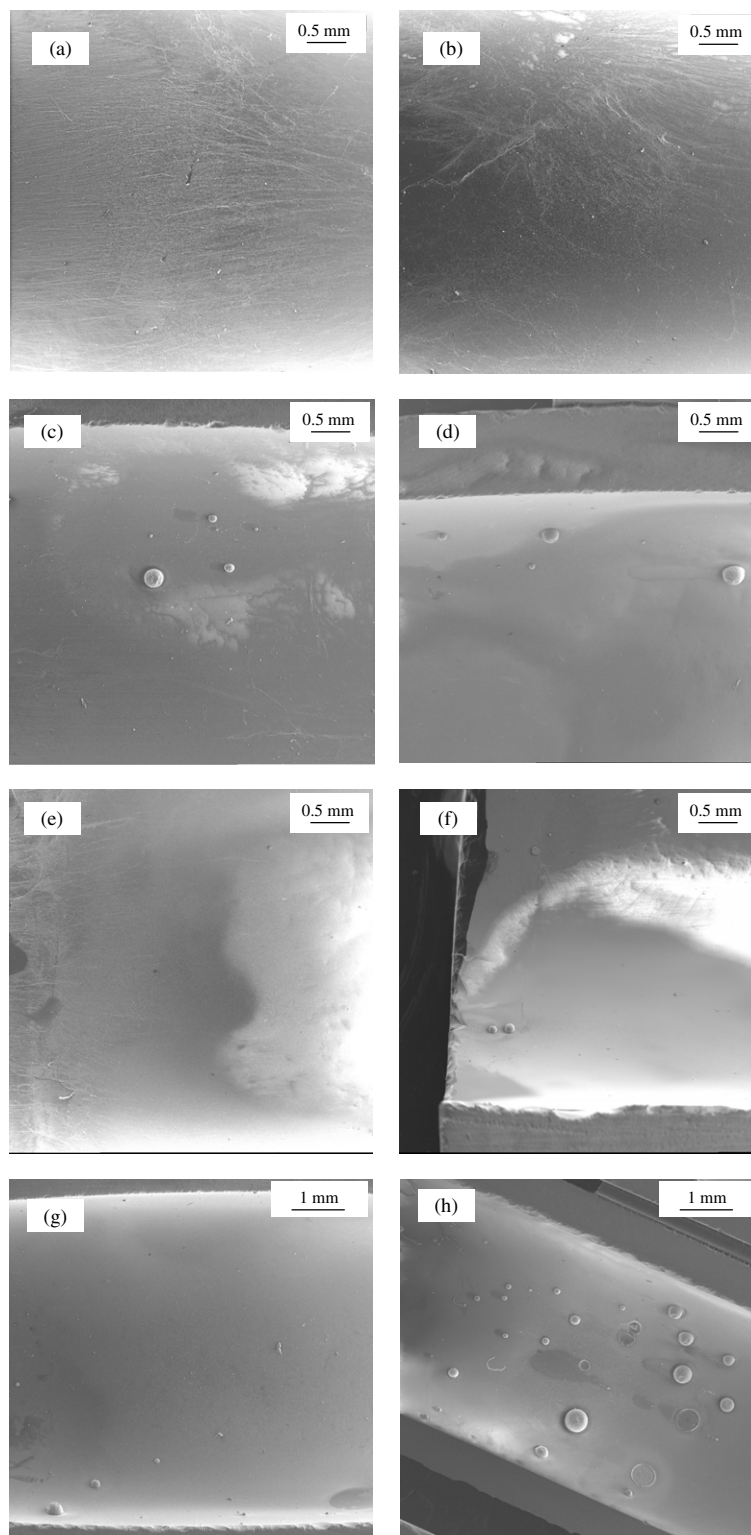


Figure 2. Vapourized elements and tiny droplets ejected from the weld pool of 304 stainless steel were captured on the inner surface of a both end open quartz tube placed co-axial with the laser beam during spot welding with 3 ms pulse duration, laser power 1067 W and spot diameter of (a) 0.625 mm, (b) 0.51 mm, (c) 0.405 mm and (d) 0.39 mm; and laser power of 1967 W and spot diameter of (e) 0.835 mm, (f) 0.651 mm, (g) 0.533 mm and (h) 0.501 mm.

co-axial to the laser beam and right above the 304 stainless steel sample tube for several cases. The EDS profile for the ejected metal droplets in figure 3 indicates the presence of Fe, Mn, Cr, Ni, Si and O elements. Of these, elements Si and

O detected by the EDS originated from the quartz tube. The remaining elements detected are the main elements in stainless steel. Therefore, the droplets shown in figure 2 originated from the molten 304 stainless steel weld pool and were then

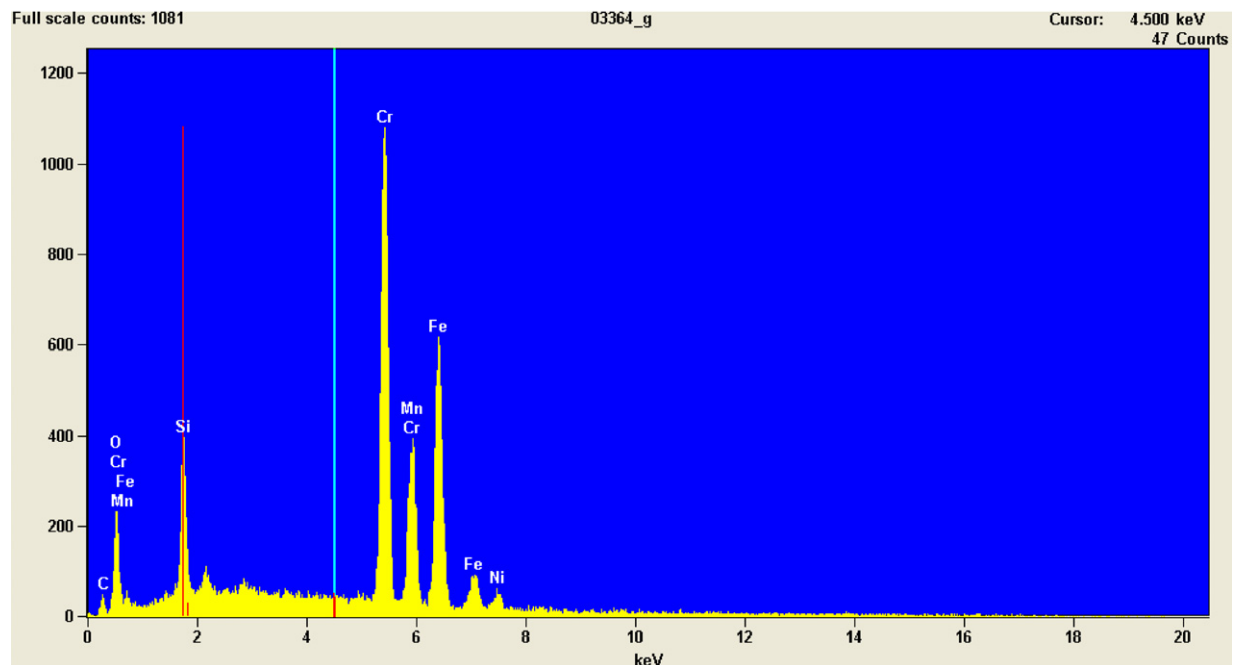


Figure 3. EDS profile for the ejected metal droplets, which were deposited on the interior wall of the quartz tube. Laser power: 1967 W, pulse duration: 3 ms and spot diameter: 0.501 mm.

(This figure is in colour only in the electronic version)

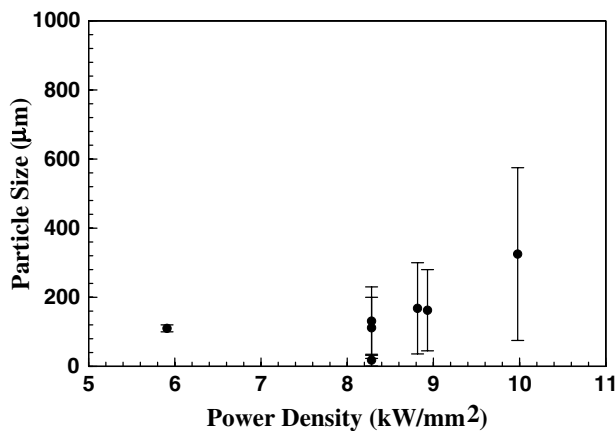


Figure 4. Effect of power density on the size of the ejected metal droplets.

deposited on the interior wall of the quartz tube during laser spot welding.

Figure 2 shows that under some welding conditions, only deposition of metal vapour was observed on the interior wall of the quartz tube, whereas both vapour condensate and ejected metal droplets were observed under other conditions. The size range of the ejected droplets was determined by optical microscopy for different welding conditions. Figure 4 shows the ejected droplet size as a function of the power density. It can be seen that the size of ejected droplets ranged from tens of micrometres to several hundred micrometres. The increase in the power density resulted in larger particle size and particle size range. With the increase in power density, both the weld pool temperature as well as the weld pool size increase. The higher recoil pressures as well as the availability of more liquid

metal are consistent with more liquid metal expulsion and larger droplets. The calculations to be presented subsequently in this paper will show that after the initiation of the pulse, the weld pool is heated for a certain duration before the liquid metal expulsion starts. Subsequently the metal expulsion takes place over a span of time until the end of the pulse. The system does not reach steady state during the metal expulsion. As a result, the ejected particles show a range of droplet sizes as observed in figure 4.

The experimental results indicated that liquid metal expulsion took place at higher laser power densities when the weld metal was heated to higher temperatures. Calculated temperature distributions along the x direction on the weld pool surface at different times for the samples A, B, C and D are shown in figure 5. The model has been previously used to calculate weld pool geometry, temperature and velocity fields during the welding of pure iron [29, 30], steel [3, 6, 31–35], aluminium alloy [5] and titanium alloy [35] under different welding conditions. The origin in figure 5 represents the location of the laser beam. The two lines in the figure indicate solidus (1697 K) and liquidus temperatures (1727 K). The thin region between these two lines is the two-phase solid–liquid mushy zone. It can be seen that the temperatures reach very high values near the laser beam axis and decrease with distance. It can also be observed that there are inflexion points close to the mushy zone, which results from the differences in the enthalpies of the solid and liquid metals. Also, with the decrease in beam radius, the temperatures increase due to higher laser power density. The calculation of temperature at different locations on the weld pool surface and at different times provides a theoretical basis in determining whether liquid metal expulsion can take place.

High temperatures result in high equilibrium vapour pressures, which tend to push the liquid metal out of the weld

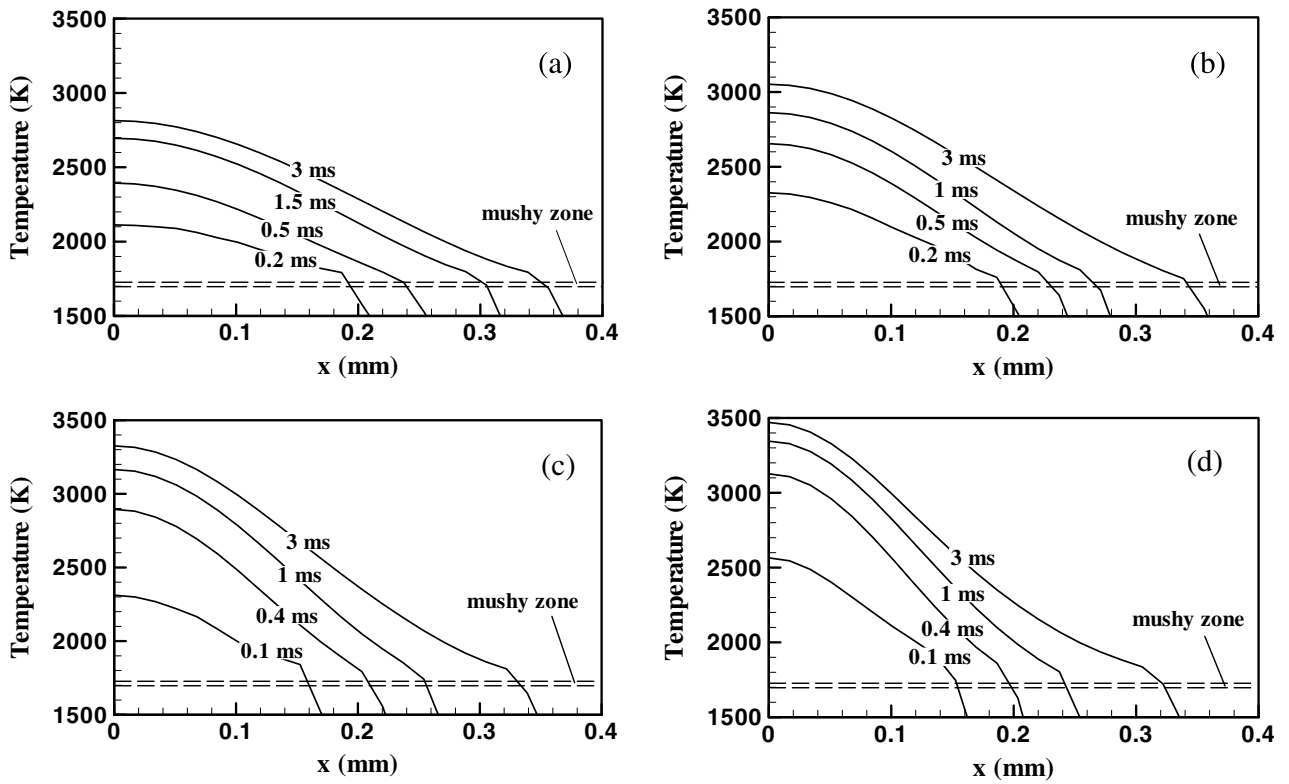


Figure 5. Distribution of temperatures on the weld pool surface at different times. Laser power: 1067 W, pulse duration: 3 ms and spot diameter: (a) 0.625 mm, (b) 0.51 mm, (c) 0.405 mm and (d) 0.39 mm.

pool. On the other hand, the surface tension force of the liquid metal holds the liquid metal in place, which tends to prevent liquid metal expulsion. When the temperature on the surface of the weld pool exceeds a critical value, the recoil force overcomes the surface tension force and liquid metal is expelled from the liquid pool. The vapour recoil force F_r and the surface tension force at the periphery F_s can be expressed by

$$F_r = 2\pi \int_0^{r_B} r \Delta P(r) dr, \quad (10)$$

$$F_s = 2\pi r_0 \sigma, \quad (11)$$

where r_B is the radial distance at which the surface temperature reaches the boiling point, ΔP is the difference between the local equilibrium vapour pressure and the atmospheric pressure and is the function of the radial distance from the beam axis, r_0 is the radial distance at which the temperature is equal to the melting point and σ is the surface tension coefficient at the melting point. Figure 6 shows the computed values of the surface tension force and vapour recoil force as a function of time during laser spot welding of 304 stainless steel. For example, in figure 6(c), it is observed that the surface tension force is higher than the recoil force at the start of the pulse. As the temperature increases with time, both the surface tension force and the recoil force increase. However, the recoil force increases faster than the surface tension force. At about 2.6 ms after the start of the pulse, the two forces are roughly equal. Further heating results in a higher recoil force than the surface tension force. When the recoil force exceeds the surface tension force, expulsion of liquid metal is anticipated. For sample A in figure 6(a), the peak temperature on the weld pool

surface is 2814 K, which is lower than the boiling point of 304 stainless steel, about 2980 K, which means that the vapour pressure is lower than one atmosphere and no expulsion of liquid metal occurs. For sample B in figure 6(b), although the peak temperature, 3052 K, exceeds the boiling point of 304 stainless steel, the recoil force is weaker than the surface tension force of the liquid metal at the periphery of the weld pool for the whole pulse duration. As a result, no liquid metal expulsion takes place. From figure 6, for samples C, D, F, G, H, the recoil force begins to exceed the surface tension force at some time during the welding process, which means that it is possible for liquid metal droplets to be ejected from the weld pool. This conclusion agrees well with experimental observations indicated in table 2, which illustrates whether the liquid metal expulsion takes place.

The experimental combinations of laser power and spot diameter that lead to liquid metal expulsion for pulse durations of 3.0 ms and 4.0 ms, respectively, are shown by a dotted line in figure 7. The points on the same dotted curve have the same laser power density, defined by laser power per unit area. It is observed that the liquid expulsion occurs above a critical laser power. For the same laser power, when the spot diameter is large, liquid metal expulsion is not observed. With the decrease in spot diameter, the intermittent expulsion occurs due to the increase in the laser power density. When the spot diameter continues to decrease, the laser power density increases and eventually significant expulsion takes place at a high laser power density. Figure 7 shows that pulse duration also has effects on liquid metal expulsion. For a 3.0 ms pulse duration, the critical laser power density for liquid metal expulsion is about 8.0 kW mm^{-2} . However, when the pulse duration is

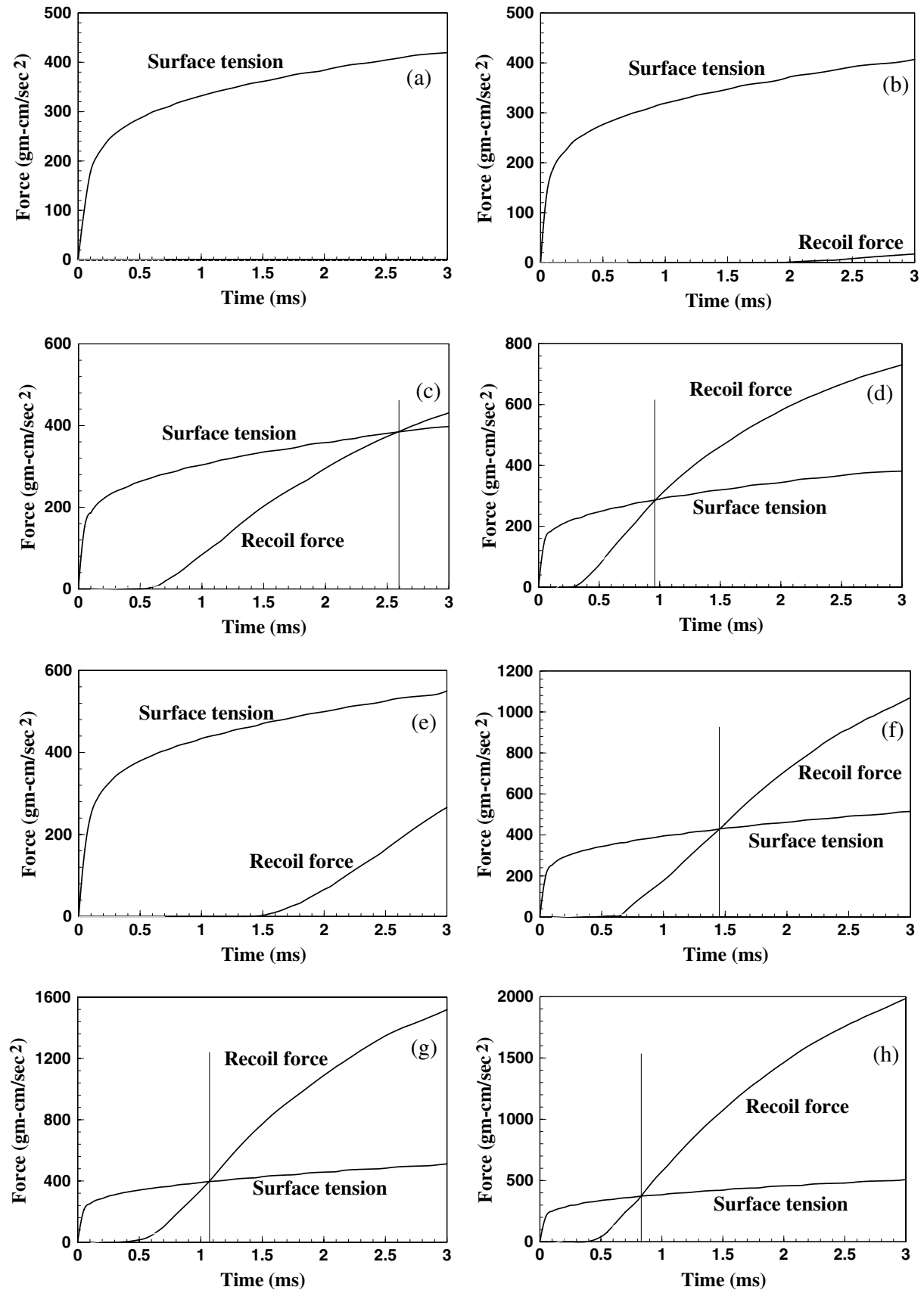


Figure 6. Recoil force and surface tension force at the periphery of the liquid pool as a function of time under the condition of 3 ms pulse duration, laser power 1067 W and spot diameter of (a) 0.625 mm, (b) 0.51 mm, (c) 0.405 mm and (d) 0.39 mm; and laser power of 1967 W and spot diameter of (e) 0.835 mm, (f) 0.651 mm, (g) 0.533 mm and (h) 0.501 mm.

Table 2. Vapour deposit and tiny droplet expulsion observed in experiments. Pulse duration: 3 ms.

Sample no.	Laser Power (W)	Spot diameter (mm)	Power density (W mm ⁻²)	Observation	Size for ejected liquid droplets (μm)
A	1067	0.625	3478	Vapour deposit only	—
B	1067	0.51	5223	Vapour deposit only	—
C	1067	0.405	8283	Vapour deposit and tiny droplet expulsion	1–35 23–200
D	1067	0.39	8932	Vapour deposit and tiny droplet expulsion	45–280
E	1967	0.835	3592	Vapour deposit only	—
F	1967	0.651	5910	Vapour deposit and tiny droplet expulsion	100–120
G	1967	0.533	8816	Vapour deposit and tiny droplet expulsion	36–300
H	1967	0.501	9978	Vapour deposit and tiny droplet expulsion	75–575

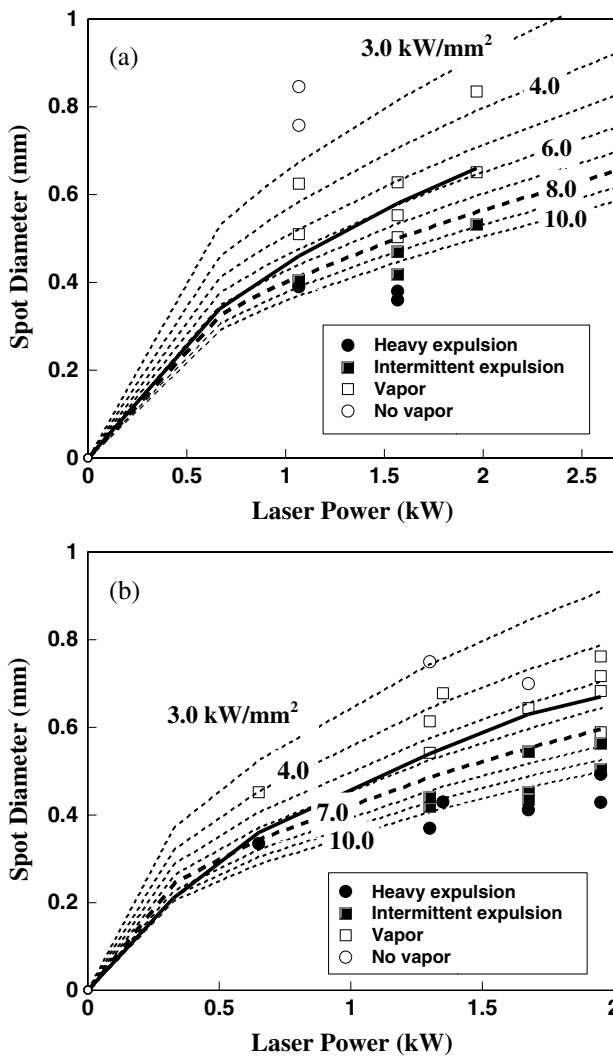


Figure 7. Liquid metal expulsion analysis data under different laser power densities for laser spot welding of 304 stainless steel. (a) 3.0 ms pulse duration and (b) 4.0 ms pulse duration.

increased to 4.0 ms, the critical laser power density decreases to about 7.0 kW mm⁻². The recoil and surface tension forces were compared to predict the critical beam diameter under different laser powers, as shown by the solid lines in figure 7.

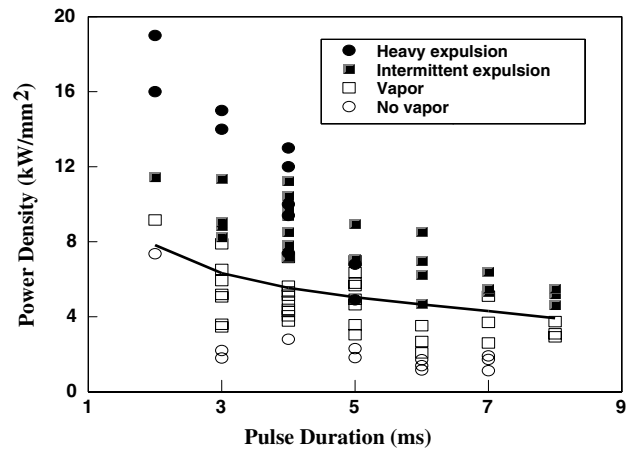


Figure 8. Analysis of liquid metal expulsion under different laser power densities and pulse durations for laser spot welding of 304 stainless steel.

The computed spot diameter and the laser power combination necessary to initiate liquid metal expulsion agreed well with experiments, indicating the accuracy of the mechanism of the liquid metal expulsion.

Figure 8 shows the extent of the liquid metal expulsion under different laser power densities and pulse durations. At a given pulse duration, higher laser power density increases the tendency of intermittent or heavy liquid metal expulsion. At 7 kW mm⁻², no vapour deposit was noticeable on the inner surface of the quartz tube for a pulse duration of 2 ms. When the pulse duration was increased to 3 ms, a coating of metal vapour condensate was found on the inner wall of the quartz tube. When the pulse duration was further increased to higher than 4 ms, intermittent or heavy expulsion of metal drops was observed. Liquid metal expulsion can take place at a lower critical power density when longer duration pulses are used, which is also predicted from the calculated results, as shown by the solid line in figure 8. The longer pulse duration allows more interaction time between the laser beam and the materials and leads to high weld pool temperatures and high recoil pressures. Therefore, liquid metal expulsion can take place at a lower laser power density when a longer pulse duration is used. Laser power density and pulse duration are the two most important parameters for the liquid metal expulsion. The results shown in

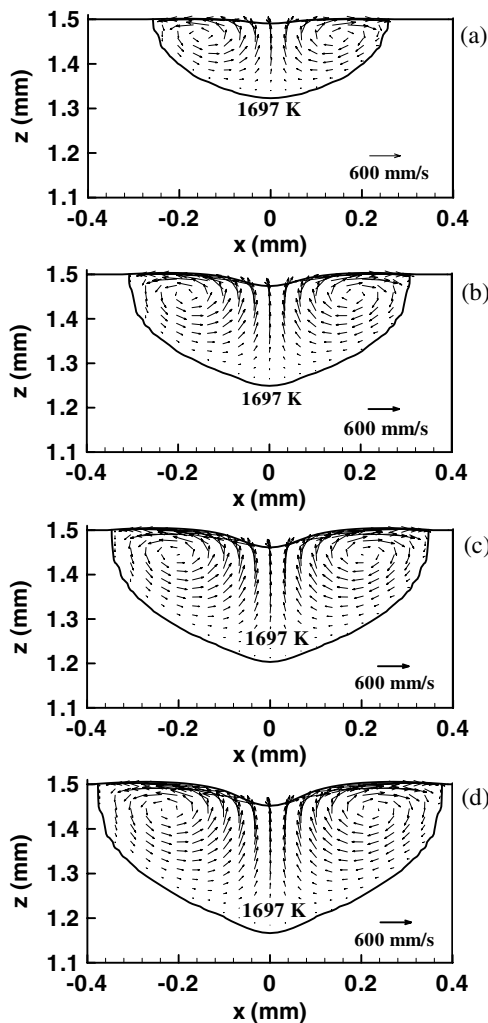


Figure 9. Temperature distribution with free surface at times of (a) 1 ms, (b) 2 ms, (c) 3 ms and (d) 4 ms. Laser power: 1300 W; pulse duration: 4 ms; spot diameter: 0.42 mm.

figures 7 and 8 provide guidance in controlling the occurrence of liquid metal ejection in laser spot welding by adjusting these two parameters.

Figure 9 shows the computed free surface profiles at different times. The sample surface is taken as the reference surface. Near the middle of the weld pool, the liquid metal is depressed due to high recoil pressure. The liquid metal displaced from the middle is transported near the boundary of the weld pool, where a hump is formed to satisfy the conservation of the total volume. With time, the recoil pressure on the weld pool increases due to higher surface temperatures. As a result, the extent of surface deformation increases with time. The dimensionless number, ratio of maximum depression, l , to the weld pool depth, d , is used to indicate the extent of surface deformation. Figure 10 shows that the ratio increases with time. The variation of l/d with the laser power density is shown in figure 11. It can be seen that the ratio increases as the laser power density increases. When the laser power density is low, the temperature is lower than the boiling point, the vapour pressure is lower than atmospheric pressure and the weld pool surface is flat. As the laser power density increases, the temperature on the weld pool surface

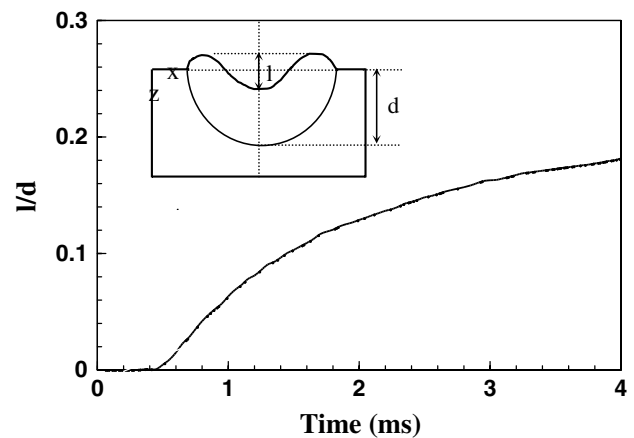


Figure 10. Computed l/d as a function of time. Laser power: 1067 W; pulse duration: 3 ms; spot diameter: 0.405 mm.

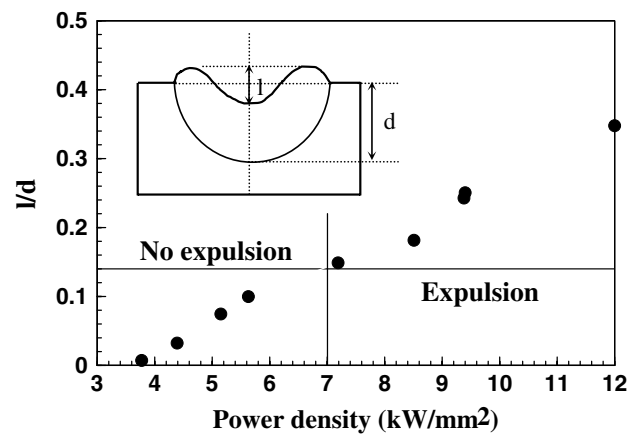


Figure 11. Variation of l/d with the laser power density. Pulse duration: 4 ms.

can become higher than the boiling point, and significant deformation of the free surface occurs. Figure 7(b) shows that the critical laser power density is 7 kW mm^{-2} for a pulse duration of 4 ms. This experimental result is in agreement with the calculations of the vapour recoil pressure and the surface tension force. The corresponding value of maximum depression of the liquid metal is about 14% of the weld pool depth from figure 11. The results in figure 11 indicate that apart from the calculations of the recoil and the surface tension force, the depression of the free surface may also serve as an indicator of liquid metal expulsion.

5. Summary and conclusions

During the laser spot welding of 304 stainless steel, liquid metal droplets are expelled from the weld pool when the peak temperature in the weld pool is very high. The liquid metal expulsion can be predicted by balancing the vapour recoil force with the surface tension force at the periphery of the liquid pool under various welding conditions. The laser power density and pulse duration are the two most important parameters for liquid metal expulsion during laser spot welding. The higher laser power density and longer pulse duration increase the

tendency of the occurrence of liquid metal expulsion. The size of the ejected droplets ranged from tens of micrometres to several hundred micrometres. The increase in the power density resulted in larger droplets and greater size range of particles. The depression of the weld centre under the recoil pressure could be used as an indicator of liquid metal expulsion during welding.

Acknowledgments

The work was supported by a grant from the US Department of Energy, Office of Basic Energy Sciences, Division of Materials Sciences, under grant number DE-FGO2-01ER45900. Portions of this work, performed at Sandia National Laboratories, were supported by the United States Department of Energy's National Nuclear Security Administration under contract DE-AC04-94AL85000. The authors would like to thank Paul Hlava for help with the experimental measurements.

References

- [1] David S A and DebRoy T 1992 *Science* **257** 497
- [2] Dunn G J, Allemand C D and Eagar T W 1986 *Metall. Trans.* **17A** 1863
- [3] Collur M M, Paul A and DebRoy T 1987 *Metall. Trans. B* **18B** 733
- [4] Cieslak M J and Fuerschbach P W 1988 *Metall. Trans. B* **19B** 319
- [5] Zhao H and DebRoy T 2001 *Metall. Trans. B* **32B** 163
- [6] Mundra K and DebRoy T 1993 *Metall. Trans. B* **24B** 145
- [7] Khan P A A, DebRoy T and David S A 1988 *Welding J.* **67** 1s
- [8] He X, DebRoy T and Fuerschbach P W 2003 *J. Phys. D: Appl. Phys.* **36** 3079
- [9] Voisey K T, Cheng C F and Clyne T W 2000 *Laser-Solid Interactions for Materials Processing (San Francisco, CA)* ed D Kumar *et al* (Warrendale, PA: Materials Research Society) p J5.6.1
- [10] Voisey K T, Kudesia S S, Rodden W S O, Hand D P, Jones J D C and Clyne T W 2003 *Mater. Sci. Eng. A* **356** 414
- [11] Lu Y F, Zheng Y W and Song W D 2000 *J. Appl. Phys.* **87** 549
- [12] Yilbas B S 1995 *J. Laser Appl.* **7** 147
- [13] Rodden W S O, Solana P, Kudesia S S, Hand D P, Kapadia P, Kowden J and Jones J D C 1999 *Int. Congr. Applications of Lasers and Electro-optics (San Diego, CA)* p 61
- [14] von Allmen M and Blatter A 1995 *Laser-Beam Interactions with Materials* (New York: Springer)
- [15] von Allmen M 1976 *J. Appl. Phys.* **47** 5460
- [16] Chan C L and Mazumder J 1987 *J. Appl. Phys.* **62** 4579
- [17] Basu S and DebRoy T 1992 *J. Appl. Phys.* **72** 3317
- [18] Semak V V, Bragg W D, Damkroger B and Kempka S. 1999 *J. Phy. D: Appl. Phys.* **32** L61
- [19] Semak V V and Matsunawa A 1997 *J. Phy. D: Appl. Phys.* **30** 2541
- [20] Brent A D, Voller V R and Reid K J 1988 *Numer. Heat Transfer* **13** 297
- [21] Patankar S V 1980 *Numerical Heat Transfer and Fluid Flow* (New York: Hemisphere Publishing Corporation)
- [22] He X, Fuerschbach P W and DebRoy T 2003 *J. Phy. D: Appl. Phys.* **36** 1388
- [23] He X, DebRoy T and Fuerschbach P W 2003 *J. Appl. Phys.* **94** 6949
- [24] Davis J R 1998 *Metals Handbook* (Materials Park, OH: ASM International)
- [25] Davis J R 1994 *ASM Specialty Handbook. Stainless Steel* (Materials Park, OH: ASM International)
- [26] ASM International Handbook Committee 1990 *Metals Handbook Volume 1. Properties and Selection: Iron, Steels, and High-performance Alloys* (Materials Park, OH: ASM International)
- [27] Peckner D and Bernstein I M 1977 *Handbook of Stainless Steels* (New York: McGraw-Hill)
- [28] Fuerschbach P W and Norris J T 2002 Beam characterization for Nd:YAG spot welding lasers *Int. Conf. Application of Lasers and Electro-Optics 2002 (Scottsdale, AZ)*
- [29] Sahoo P, Collur M M and DebRoy T 1988 *Metall. Trans. B* **19B** 967
- [30] Paul A and DebRoy T 1988 *Metall. Trans. B* **19B** 851
- [31] Zhang W, Roy G, Elmer J and DebRoy T 2003 *J. Appl. Phys.* **93** 3022
- [32] He X, Elmer J and DebRoy T 2005 *J. Appl. Phys.* **97** 84909
- [33] Zhang W, DebRoy T and Elmer J W 2005 *Sci. Technol. Weld. Joining* **10** 574
- [34] Zhang W, DebRoy T, Palmer T A and Elmer J W 2005 *Acta Mater.* **53** 4441
- [35] Yang Z, Sista S, Elmer J W and DebRoy T 2000 *Acta Mater.* **48** 4813